Step Edge Sputtering Yield at Grazing Incidence Ion Bombardment

Henri Hansen,* Celia Polop, and Thomas Michely
I. Physikalisches Institut, RWTH Aachen, D-52056 Aachen, Germany

Andreas Friedrich and Herbert M. Urbassek
Fachbereich Physik, Universität Kaiserslautern, D-67653 Kaiserslautern
(Received 12 February 2004; published 18 June 2004)

The surface morphology of Pt(111) was investigated by scanning tunneling microscopy after 5 keV Ar^+ ion bombardment at grazing incidence in dependence of the ion fluence and in the temperature range between 625 and 720 K. The average erosion rate was found to be strongly dependent on the ion fluence and the substrate temperature during bombardment. This dependence is traced back to the variation of step concentration with temperature and fluence. We develop a simple model allowing us to determine separately the constant sputtering yields for terraces and for impact area stripes in front of ascending steps. The experimentally determined yield of these stripes—the step-edge sputtering yield—is in excellent agreement with our molecular dynamics simulations performed for the experimental situation.

DOI: 10.1103/PhysRevLett.92.246106 PACS numbers: 79.20.Rf, 31.15.Qg, 68.37.Ef, 68.47.De

Grazing incidence ion bombardment may be used for smoothing of surfaces [1,2] and of growing films [3] as well as for the formation of regular nanogrooves [4], ripple [5], and dot [6] patterns. Measuring the reflected ion current or the related sample current during grazing incidence ion bombardment allows us to obtain information on surface structure and even surface morphological evolution during epitaxial growth [7–10]. The origin of all these applications is the selective interaction of the ion beam with the surface topology. Focusing to the case of crystalline surfaces this statement specializes for most applications to a highly selective interaction of grazing incidence ions with atomic steps. Because of the only small perpendicular kinetic energy of the grazing incident ions they are reflected from the atomically smooth terraces with a high degree of perfection. However, grazing incidence ions impinging on rising steps are scattered at large angles, give rise to significant momentum and energy transfer to the substrate, and thus cause sputtering. As a consequence, unlike in normal incidence ion bombardment [11,12], at grazing incidence the areal averaged sputtering yield $\overline{Y}$ is no more a nearly constant quantity: The variation of the step density with fluence F and temperature T makes this quantity a strong function of F and T. Motivated by previous molecular dynamics simulations [13], here we introduce a new concept for the description of ion erosion at grazing incidence, attributing separate constant sputtering yields to terraces (Y^{terr}) and steps (Y^{step}) such that $\overline{Y}$ may be written as $\overline{Y} = \alpha Y^{\mathrm{step}} + (1-\alpha)Y^{\mathrm{terr}}$, where α is a measure of the step density. This concept allows us for the first time to measure the step-edge sputtering yield Y^{step}, which is in very good agreement with our molecular dynamics simulations.

The experiments were performed in an ultrahigh vacuum variable temperature scanning tunneling microscopy (STM) apparatus with a base pressure in the 10^{-11} mbar range. Sample cleaning was accomplished by cycles of ion bombardment and flash annealing to 1273 K. For the grazing incidence ion experiments the clean surface was exposed to a flux of 1.6×10^{16} ions/m^2 of 5 keV Ar^+ ions incident along the $[\bar{1}\,\bar{1}\,2]$ direction at an angle of $\vartheta = 83°$ to the surface normal at various temperatures and for various exposure times. For simplicity, in the following not only the removed material Θ but also the ion fluence F (the product of ion flux and exposure time) is specified in monolayers (ML), where 1 ML $= 1.504 \times 10^{19}$ atoms(ions)/m^2. After bombardment the sample was quenched to room temperature and imaged by STM.

A sequence of experiments with increasing fluences at 720 K is visualized by the STM topographs in Figs. 1(a)–1(d). At this bombardment temperature subsurface damage anneals rapidly to the surface [14] such that the removed material is represented by surface vacancies, which are aggregated in the form of monolayer deep vacancy islands. Because of rapid edge diffusion and step adatom detachment [15], the island shapes are close to their threefold symmetric equilibrium shape. As expected, the quantitative analysis in Fig. 1(e) shows a monotonic increase of the removed and thus sputtered material Θ with F. However, the slope of the increase—corresponding to $\overline{Y}$—is nonuniform, with a small initial $\overline{Y}$ during the island nucleation phase, a maximum around $F = 1$ ML and a decreasing $\overline{Y}$ as island coalescence takes place [compare Fig. 1(d)]. To first approximation the instantaneous $\overline{Y}$ appears thus to be proportional to the concentration of step atoms on the surface.

A second sequence of experiments shown in Figs. 2(a)–2(d) visualizes the dependence of $\overline{Y}$ on T for a fixed ion fluence of $F = 0.5$ ML. As expected from nucleation theory, the vacancy island density increases with decreasing temperature due to a decreasing mobility of surface

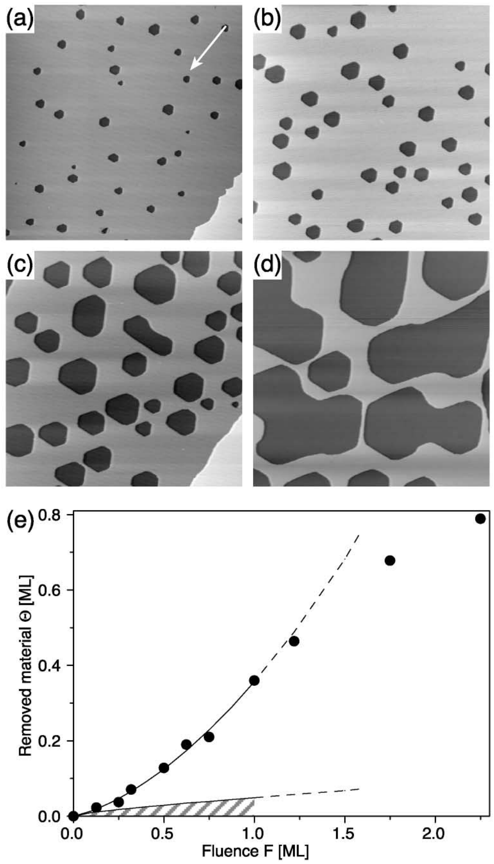

FIG. 1. (a)–(d) STM topographs of Pt(111) after 5 keV Ar^+ ion bombardment at 720 K. The ion fluences are (a) 0.25, (b) 0.50, (c) 1.00, and (d) 1.75 ML. The topograph size is always2450 Å × 2450 Å. (e) Plot of the removed amount Θ versus the ion fluence F. Full circles represent the experimental data, while the full line is the best fit of the geometric model to the experimental data up to fluences of 1.0 ML (see text). For larger fluences, beyond the limits of applicability, the best fit results of the geometric model are represented by a dashed line. The hashed area represents the removed material due to impacts on the terrace area A^{terr}.

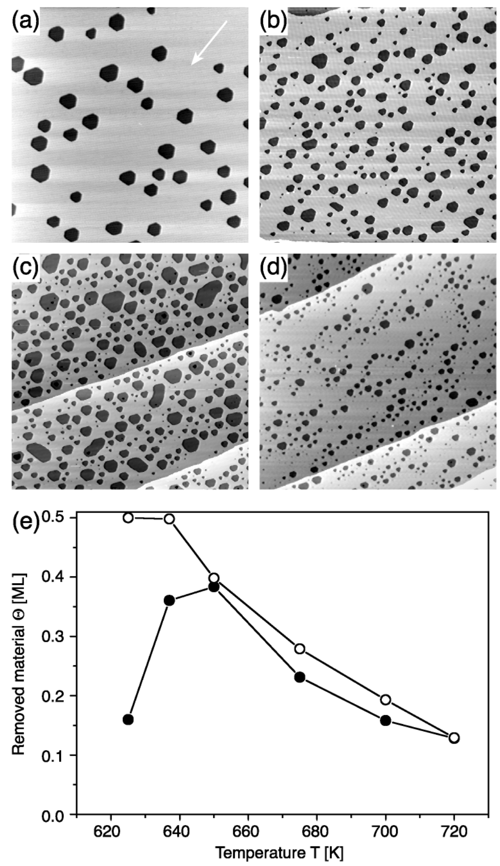

FIG. 2. (a)–(d) STM topographs after the irradiation with a fluence of 0.5 ML at (a) 720, (b) 675, (c) 650, and (d) 625 K, respectively. The ion beam is incident along the direction indicated by the white arrow in (a). The topograph size is always 2450 Å × 2450 Å. (e) Plot of the removed amount Θ versus the bombardment temperature T. Full circles represent the experimental data, while the open circles are the prediction of the model based on the Y^{terr} and Y^{step} as determined from the fluence dependence of Θ. Lines are guides to the eye.

vacancies and small vacancy clusters. More interesting is the increase in Θ with decreasing T from 720 [Fig. 2(a)] to 650 K [Fig. 2(c)]. Below 650 K Θ decreases again below its maximum value as apparent from the quantitative analysis of Fig. 2(e). The increase of Θ with a decrease of T from 720 to 650 K may again be rationalized by the higher average step density at lower temperatures, which is caused by the higher island number density. The interpretation of the decrease of Θ below 650 K is straightforward. Certainly below 650 K the surface vacancy island coverage does no more represent the entire removed material, as subsurface vacancies and vacancy clusters created during the bombardment do not anneal completely to the surface [14]. Additional factors for the decrease of Θ below 650 K are discussed below.

In order to obtain a quantitative understanding of the evolution of Θ (and thus $\overline{Y}$) we resort to the geometric model developed on the basis of molecular dynamics simulations for Xe^+ ions at grazing incidence along the $[\bar{1}\,\bar{1}\,2]$ direction impinging on ascending dense packed steps oriented along the $\langle 110 \rangle$ [13]. Ions geometrically hitting the ascending step of height Δh, i.e., that enter at a distance within $[-x_c, 0]$ the level of the upper terrace [dashed line in Fig. 3(a)] were found to have a significant sputtering yield. We denote its average in the interval $[-x_c, 0]$ in the following by Y^{step}. The critical distance x_c can be calculated from Fig. 3(a) to be $x_c = 2\Delta h \tan\vartheta$, where $\vartheta = 83°$ is the ion impact angle, which amounts to $x_c = 36.9$ Å in the present case. With $\Delta x = 2.40$ Å being the spacing of the atomic rows in the $[\bar{1}\,\bar{1}\,2]$ direction, this corresponds to a distance of $x_c/\Delta x = 15.4$ atomic rows. Ions not hitting the ascending step but the terrace were found to have a zero yield at $T = 0$. This is reasonable since the perpendicular energy, $E\cos^2\vartheta$, amounts to only 74 eV. Though still small, due to vibrations at finite

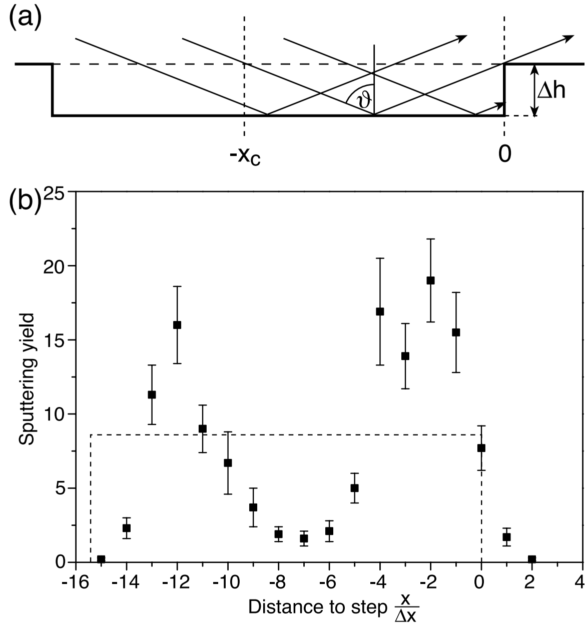

FIG. 3. (a) Schematic side view of a surface with a step. In this geometric model ions entering the upper terrace level (dashed line) between $[-x_c, 0]$ hit the ascending step either directly or indirectly by reflection at the lower terrace. (b) Dependence of the sputtering yield calculated by molecular dynamics as a function of the distance from the step location at x_c. The dashed line is the average in the impact distance interval $[-x_c, 0]$ of the geometric model. $x/\Delta x$ measures the distance of the ion impact point to the step edge in units of the spacing of dense packed atomic rows on the (111) surface.

temperatures and the possible existence of point defects at the surface their yield will be nonzero in general and we assign in the following a yield Y^{terr} to them. The molecular dynamics simulation performed for 5 keV Ar^+ ions impinging along the $[\bar{1}\,\bar{1}\,2]$ direction on an ascending dense packed step on Pt(111) directly verify the validity of the above model for the present case. The simulation data are shown in Fig. 3(b). Within the step-edge zone of width $[-x_c, 0]$ the yield significantly deviates from zero with an average value of $Y^{\mathrm{step}} = 8.3$ denoted by the dashed line. The two maxima visible in Fig. 3(b) indicate the impact zones, where the impinging ion either directly $[x \cong (-2 \ldots -4)\Delta x]$ or after reflection from the lower terrace $[x \cong (-11 \ldots -13)\Delta x]$ collides with the step-edge atom and thereby transfers a high amount of energy to near-surface atoms, leading to sputtering. In an impact zone around $-x_c/2$, the sputtering yield, however, is quite small. In this case the projectile has a good chance to be channeled immediately under the top monolayer of the upper terrace, and thus has least interaction with the step-edge atom. Here, a finite target temperature would tend to smoothen the structures visible in Fig. 3(b). We note that each data point in Fig. 3(b) is the averaged yield for 25 impacts. Further details of the simulation are given in Ref. [13].

For a large, compact island with a lateral dimension l in the direction normal to the impinging ion beam the impact area a^{step} is to good approximation $a^{\mathrm{step}} \approx l x_c$, if $l \gg x_c$. However, for small, compact islands this approximation overestimates a^{step}, as a^{step} becomes larger than the island area. Therefore, for small, compact islands we approximate a^{step} by the island area. For the geometry present in the experiments described above with hexagonal islands this is the case if $l \leq 8/(3\sqrt{3})x_c$. In the further analysis we denote the total area fraction of island impact areas by A^{step}. The total area fraction of the remaining terrace areas with the low yield Y^{terr} is then simply given by $A^{\mathrm{terr}} = 1 - A^{\mathrm{step}}$.

During the surface morphological evolution caused by ion bombardment the step-edge concentration and consequently the ratio between A^{step} and A^{terr} are subject to large changes. The fluence dependent average sputtering yield $\overline{Y}$ is then given by the following differential equation:

$$\overline{Y} = \frac{d\Theta}{dF} = Y^{\mathrm{step}} A^{\mathrm{step}} + Y^{\mathrm{terr}}(1 - A^{\mathrm{step}}). \qquad (1)$$

To solve (1) we make the following simplifying assumptions: (i) all islands nucleate at $t = 0$; (ii) the islands grow with the same speed and have the same size at all times; (iii) the island density stays constant.

Using the approximations for a^{step} introduced above and as experimental input data the vacancy island number densities determined from the STM topographs, Eq. (1) can be applied to reproduce the experimental data. The full line in Fig. 1(e) represents the best fit of (1) to the measurements at 720 K for fluences up to 1.0 ML. For larger fluences coalescence becomes noticeable [compare Fig. 1(d)]. In the coalescence regime the model is no longer applicable, and the extension of the fit into this regime is represented by the dashed line in Fig. 1(e). The best fit parameters are $Y^{\mathrm{step}} = 8.4$ and $Y^{\mathrm{terr}} = 0.08$. A three-dimensional representation of the sum χ of the quadratic deviations of the fitted data from the experiment as a function of Y^{terr} and Y^{step} allows us to estimate the errors for Y^{step} and Y^{terr} to be 1.5 and 0.03, respectively. We note that our experimental results are in excellent agreement with the molecular dynamics simulations [compare Fig. 3(b)], which yield $Y^{\mathrm{step}} = 8.3$ and $Y^{\mathrm{terr}} = 0$ at 0 K.

The total removed material Θ can be divided into material Θ^{terr} removed by ions impinging on A^{terr} and material Θ^{step} removed by ions impinging on A^{step}. The hashed area in Fig. 1(e) represents $\Theta^{\mathrm{terr}} = Y^{\mathrm{terr}} \times \int_0^F df\,[1 - A^{\mathrm{step}}(f)]$. It grows nearly linearly with time as A^{terr} stays close to 1 during the entire experiment. Θ^{step}, the difference between the hatched area and the best fit grows much stronger than linearly. Assuming $Y^{\mathrm{terr}} = 0$, once initial nuclei are given, Θ^{step} grows quadratically as the increase in Θ with F is proportional to $\sqrt{\Theta}$.

In order to test the validity of the model, we apply the values obtained for Y^{terr} and Y^{step} from the fluence dependence of Θ at 720 K to predict the temperature dependence of Θ for the fixed fluence $F = 0.50$ ML. The predicted dependence of the removed amount Θ on T is shown in Fig. 2(e) as open circles. The agreement of experiment and prediction is quite good down to 650 K. Below 650 K the measured Θ decreases again, while the calculated one goes into saturation. The constancy of the calculated Θ for low temperatures can be understood as follows: At these low temperatures the island number density is so high such that the average island size stays below $l \leq 8/(3\sqrt{3})x_c$ during the entire bombardment time. As described above, therefore the area fraction A^{step} in (1) is taken to be identical to the total area fraction of the islands, which is thus no longer dependent on the island number density and therefore on the temperature.

The experimentally observed decrease of the vacancy island area below 650 K is expected, as below 650 K bombardment induced subsurface vacancies no more anneal completely to the surface [14]. However, there are additional possible reasons why our model might deviate from the measurements for temperatures below 650 K. As can be seen from Fig. 2, the island size distribution becomes broader towards lower temperatures, making our simplifying assumptions about nucleation at $t = 0$ and identical island sizes crude. Moreover, at 625 K correlations in the positions of the vacancy islands become noticeable: Islands appear to be partly aligned along the ion beam. One possible explanation for this observation is that at 625 K step-edge diffusion is no longer efficient enough to ensure a compact island shape during bombardment, counteracting the highly anisotropic removal of material at the exposed ascending step. Therefore, during the bombardment the islands might be elongated along the beam direction—thereby having a much smaller area fraction A^{step} than assumed in our calculation—while after switching off the ion beam and during the finite cool down time the elongated islands pinch off into several parts [16]. In this scenario the correlations in the island positions at 625 K could indicate the onset of a transition from a diffusion dominated to a bombardment dominated regime of morphological evolution [5] and thus to the onset of ripple formation. Experiments are under way to clarify this issue.

In conclusion, we demonstrated experimentally that unlike in normal incidence ion bombardment, at grazing incidence the average sputtering yield $\overline{Y}$ is strongly fluence and temperature dependent. This dependence may be rationalized by attributing separate constant yields Y^{terr} and Y^{step} to terraces and impact area stripes in front of ascending steps exposed to the ion beam, respectively. Based on these assumptions, we derive for the first time a step-edge sputtering yield, which amounts to $Y^{\text{step}} = 8.4 \pm 1.5$ for 5 keV Ar^+ incident along the $[\bar{1}\,\bar{1}\,2]$ direction at $\vartheta = 83^{\circ}$ on Pt(111). This value is in excellent agreement with our molecular dynamics simulations of the experimental situation which yield $Y^{\text{step}} = 8.3$ as the average within the step impact stripe. Moreover, we confirmed the expected high selectivity of step-edge sputtering at grazing incidence ion bombardment. For the experimental conditions used here, the step-edge yield exceeds the terrace yield by a factor of 100. The measurements presented here may be a first step towards a quantitative and atomistic modeling of surface morphological evolution and ripple formation under grazing incidence ion bombardment.

We acknowledge useful discussions with Wulf Wulfhekel, Herbert Wormeester, and Bene Poelsema, the critical reading of the manuscript by Sebastian Meßlinger and Georgiana Stoian, and financial support by the Deutsche Forschungsgemeinschaft via the project "Streifender Ionenbeschuss auf Metalloberflächen."

*Electronic address: hansen@physik.rwth-aachen.de

[1] M. Wißing, M. Batzill, and K. J. Snowdon, Nanotechnology **8**, 40 (1997).
[2] J. G. C. Labanda, S. A. Barnett, and L. Hultman, J. Vac. Sci. Technol. B **16**, 1885 (1998).
[3] K. C. Ruthe and S. A. Barnett, Surf. Sci. Lett. **538**, L460 (2003).
[4] S. van Dijken, D. de Bruin, and B. Poelsema, Phys. Rev. Lett. **86**, 4608 (2001).
[5] S. Rusponi, G. Costantini, F. Buatier de Mongeot, C. Boragno, and U. Valbusa, Appl. Phys. Lett. **75**, 3318 (1999).
[6] F. Frost, A. Schindler, and F. Bigl, Phys. Rev. Lett. **85**, 4116 (2000).
[7] R. Pfandzelter, T. Bernhard, and H. Winter, Phys. Rev. Lett. **90**, 036102 (2003).
[8] M. H. Langelaar and D. O. Boerma, Surf. Sci. **436**, 237 (1999).
[9] R. Pfandzelter, T. Igel, and H. Winter, Phys. Rev. B **62**, R2299 (2000).
[10] P. M. De Luca, K. C. Ruthe, and S. A. Barnett, Phys. Rev. Lett. **86**, 260 (2001).
[11] T. J. Colla and H. M. Urbassek, Nucl. Instrum. Methods Phys. Res., Sect. B **117**, 361 (1996).
[12] M. Morgenstern, *Jül-Bericht 3269* (Forschungszentrum Jülich, Jülich, 1996), p. 60 ff.
[13] A. Friedrich and H. M. Urbassek, Surf. Sci. **547**, 315 (2003).
[14] T. Michely and G. Comsa, Nucl. Instrum. Methods Phys. Res., Sect. B **82**, 207 (1993).
[15] T. Michely, M. Kalff, G. Comsa, M. Strobel, and K.-H. Heinig, Phys. Rev. Lett. **86**, 2589 (2001).
[16] W. W. Pai, J. F. Wendelken, C. R. Stoldt, P. A. Thiel, J. W. Evans, and D.-J. Liu, Phys. Rev. Lett. **86**, 3088 (2001).